

Single-beam leaky-wave antenna with wide scanning angle and high scanning rate based on spoof surface plasmon polariton

Huan Jiang(蒋欢), Xiang-Yu Cao(曹祥玉), Tao Liu(刘涛), Liaori Jidi(吉地辽日), and Sijia Li(李思佳)
Citation: Chin. Phys. B, 2022, 31 (**10**): 104101. DOI: 10.1088/1674-1056/ac5881
Journal homepage: http://cpb.iphy.ac.cn; http://iopscience.iop.org/cpb

What follows is a list of articles you may be interested in

Design method of reusable reciprocal invisibility and phantom device

Cheng-Fu Yang(杨成福), Li-Jun Yun(云利军), and Jun-Wei Li(李俊玮)
Chin. Phys. B, 2022, 31 (**8**): 084101. DOI: 10.1088/1674-1056/ac6166

Goos-Hänchen and Imbert-Fedorov shifts in tilted Weyl semimetals

Shuo-Qing Liu(刘硕卿), Yi-Fei Song(宋益飞), Ting Wan(万婷), You-Gang Ke(柯友刚), and Zhao-Ming Luo(罗朝明)
Chin. Phys. B, 2022, 31 (**7**): 074101. DOI: 10.1088/1674-1056/ac4e03

A multi-frequency circularly polarized metasurface antenna array based on quarter-mode substrate integrated waveguide for sub-6 applications

Hao Bai(白昊), Guang-Ming Wang(王光明), Xiao-Jun Zou(邹晓鋆), Peng Xie(谢鹏), and Yi-Ping Shi(石一平)
Chin. Phys. B, 2022, 31 (**5**): 054102. DOI: 10.1088/1674-1056/ac373b

Switchable directional scattering based on spoof core—shell plasmonic structures

Yun-Qiao Yin(殷允桥), Hong-Wei Wu(吴宏伟), Shu-Ling Cheng(程淑玲), and Zong-Qiang Sheng(圣宗强)
Chin. Phys. B, 2022, 31 (**5**): 054101. DOI: 10.1088/1674-1056/ac3503

Spoof surface plasmon polaritons excited leaky-wave antenna with continuous scanning range from endfire to forward

Tao Zhong(钟涛), Hou Zhang(张厚)
Chin. Phys. B, 2020, 29 (**9**): 094101. DOI: 10.1088/1674-1056/ab9c00

Single-beam leaky-wave antenna with wide scanning angle and high scanning rate based on spoof surface plasmon polariton

Huan Jiang(蒋欢)[1,†], Xiang-Yu Cao(曹祥玉)[1,2,‡], Tao Liu(刘涛)[1], Liaori Jidi(吉地辽日)[1], and Sijia Li(李思佳)[1,2]

[1] *Information and Navigation College, Air Force Engineering University, Xi'an* 710077, *China*

[2] *Shaanxi Key Laboratory of Artificially-Structured Functional Materials and Devices, Air Force Engineering University, Xi'an* 710051, *China*

(Received 6 January 2022; revised manuscript received 9 February 2022; accepted manuscript online 25 February 2022)

We propose a single-beam leaky-wave antenna (LWA) with a wide-scanning angle and a high-scanning rate based on spoof surface plasmon polariton (SSPP) in this paper. The SSPP transmission line (TL) is etched with periodically arranged circular patches, which converts the slow-wave mode into the fast-wave region for radiation. The proposed LWA is designed, fabricated, and tested. The simulated results imply that the proposed LWA not only achieves a high radiation efficiency of about 81.4%, and a high scanning rate of 12.12, but also has a large scanning angle of 176° over a narrow operation bandwidth of 8.3–9.6 GHz (for $|S_{11}| < -10$ dB). In addition, the simulated average gain of the LWA can reach as high as 10.9 dBi. The measured scanning angle range is 175° in the operation band of 8.2–9.6 GHz, and the measured average gain is 10.6 dBi. The experimental results are consistent with the simulation, validating its performance. An antenna with high radiation efficiency, wide scanning angle range, and high scanning rate has great potential for application in radar and wireless communication systems.

Keywords: spoof surface plasmon polariton (SSPP), leaky wave antenna, wide scanning angle, high scanning rate

PACS: 41.20.Jb, 52.35.Hr **DOI:** 10.1088/1674-1056/ac5881

1. Introduction

Improving sensor detection and determining the accuracy and effectiveness of the target is a perennial challenge in radar applications.[1–5] The scanning-rate (SR) represents the sensitivity of radiation direction with frequency change. We prefer to design a leaky-wave antenna, which takes advantage of a narrower bandwidth to cover a larger scanning range. In recent years, the characteristics of LWAs based on the SSPP TL, with its simple structure, frequency scanning characteristics, and compatibility with planar circuits, have attracted significant attention.

The surface plasmon polariton (SPP) is a mixed excited state, propagating along the medium-metal interface generated during the interaction of light with a metal, and exhibiting a highly confined surface wave in the medium outside the metal.[6] The spoof surface plasmon polariton (SSPP) is the analogous extension of the SPP concept in the low-frequency band. When electromagnetic (EM) waves interact with the artificial EM medium, a kind of hybrid surface EM mode is generated at the medium interface. Its characteristic subwavelength, enhancement of the local field, and nonlinear dispersion curve offer significant application value in the design of antennas,[7] filters,[8] TLs[9] etc.[10–19]

The EM wave propagates in the form of a slow wave in the antenna, and the propagation speed of the slow wave is below that of an EM wave in free space. Slow waves cannot radiate into space directly. However, when an EM wave's propagation speed is higher than that in free space, it radiates in the form of a fast wave. To create this radiation effect in the antenna requires a progression from slow wave to fast wave. However, the conversion of a slow wave confined in the SSPP TL into a fast wave, so as to generate radiation of the frequency scanning beams, represents a technical problem with regard to SSPP-based antennas, which must be resolved. The first method involves periodically modulating the SSPP TL, so that EM waves are released into the fast wave region.[10–12] The maximum scanning angle that can be achieved in this way is 123°.[11] In view of the limitation whereby general SSPP LWAs can only radiate linearly polarized waves, Ref. [12] proposed that the SSPP unit could be rotated 45°, and the surface impedance could be controlled by changing the depth of the groove, creating an antenna adaptable to any type of polarization mode.

To realize the leaky-wave, the second method introduces periodic perturbations by periodically arranging patches around the TL, which couple the EM waves to the patches to form a fast wave pattern matching the spatial waves for beam scanning in vacuum. In Ref. [13], the antenna was composed of two rows of circular patches placed on both sides of the SSPP TL, covering an angle of 83° from 9.2 GHz to 16 GHz. In Ref. [14], an antenna based on the glide-symmetry Goubau line covers a range of 145° with high-order harmonic radiation

†Corresponding author. E-mail: huan_er_ya@163.com

‡Corresponding author. E-mail: xiangyucaokdy@163.com

© 2022 Chinese Physical Society and IOP Publishing Ltd

within 6.3% bandwidth, and achieves a very high scanning rate. However, this antenna fails to radiate efficiently, with an average radiation efficiency of only 26%. In the design of LWAs with a high scanning rate, there is always a trade-off between scanning rate and efficiency.

There are other methods of achieving frequency scanning radiation. In Ref. [15], an antenna based on a substrate integrated waveguide (SIW) realizes 35° beam scanning in a narrow band of 3%. However, due to the symmetry of its design structure, this antenna also exhibits the stop-band problem common to traditional LWAs. This inability to realize broadside radiation is a key limitation of continuous wide-angle scanning. In Ref. [16], the SSPP-based antenna used periodic holes etched in the CPW to generate waves in the higher-order SSPP mode, capable of covering a wide scanning angle of 129°, while the low scanning rate caused by an operating bandwidth of 11.7–50 GHz is not expected. Therefore, it is necessary to design a compact antenna with a wide scanning angle, a high scanning rate, and high radiation efficiency.

In this paper, a single beam SSPP-based LWA is proposed, whose compact structure can readily be fabricated for practical applications. The stop-band effect is suppressed, and the scanning range is enlarged. By adjusting the periodic modulation, the frequency band of the antenna tends to be near the cutoff frequency, exhibiting a higher scanning rate. The antenna achieves a high scanning rate of 12.12, and a efficiency of 81.4%. Its scanning angle of 176° represents the largest among antennas of the same type, and its average gain is as much as 10.9 dBi in the working frequency band. This proposed antenna based on SSPP demonstrates outstanding performance.

2. Antenna structure and design

The geometrical configuration of the proposed leaky-wave antenna is shown in Fig. 1. The SSPP TL is introduced on the middle layer. A series of circular patches are placed on the top and bottom layer as radiating elements. The layers are filled with F4BM-2, where the dielectric constant is $\varepsilon_r = 2.65$, the loss tangent is $\tan\delta = 0.001$, and the thickness of the single-layer medium is $t_h = 1$ mm. The overall size of the antenna $L \times W = 35.6\ \text{mm} \times 400\ \text{mm}$.

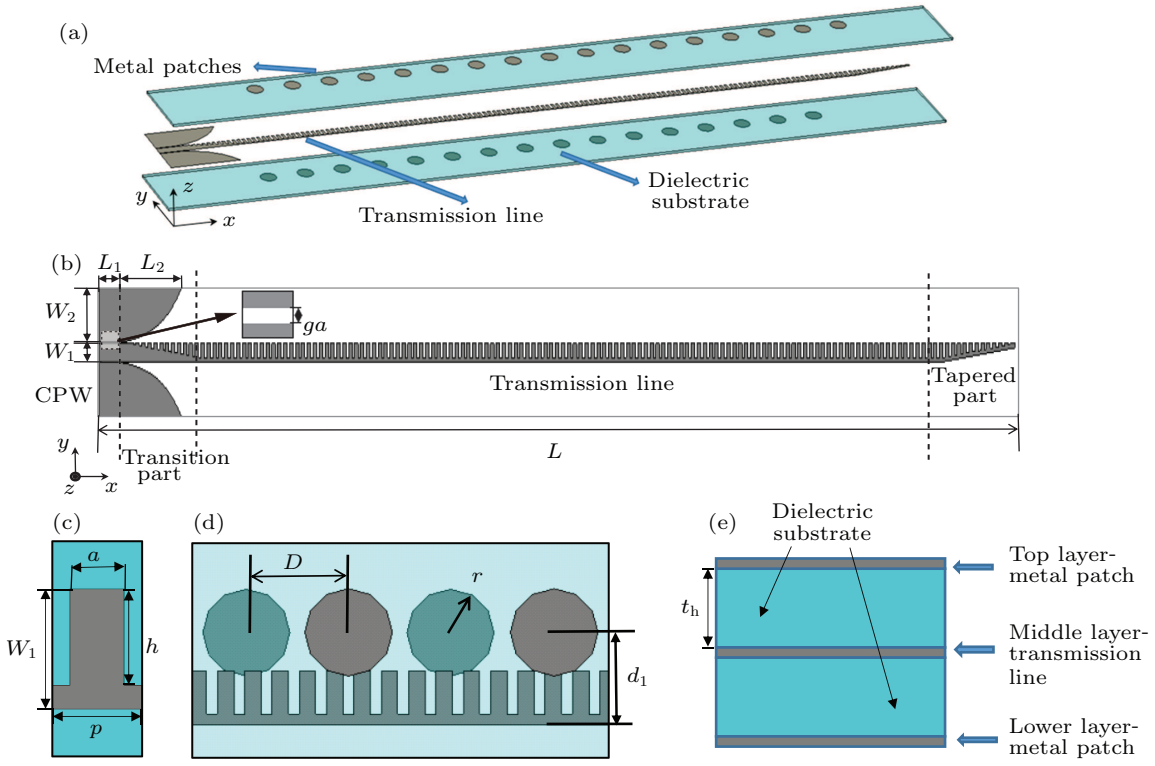


Fig. 1. Geometry of the proposed LWA. (a) Perspective view. (b) Feeding layer. (c) TL unit. (d) Radiating elements. (e) Multilayer layout.

In the middle layer, the left-hand end is fed via a coplanar waveguide (CPW) measuring $L_1 = 10$ mm. The smooth groove gradient structure is connected with TL to match the input impedance, reduce reflections, and increase the efficiency of the antenna radiation.

The exponential-shaped ground sides are conducive to an efficient matching in broadband as $y = f(x) = C_1 e^{\alpha x} + C_2$, where $\alpha = 0.1$, $C_1 = W_2/(e^{\alpha L_2} - 1)$, $C_2 = -W_2/(e^{\alpha L_2} - 1) + ga + W_1/2$ and the coordinate origin is set at the beginning of the transition. Reference [17] shows that this tapered structure forms a good bridge with which to connect the CPW, with 50 Ω impedance and SSPP TL in the microwave fre-

quency, converting the guided waves to the slow wave mode bounded in the SSPP TL, and demonstrating high efficiency in the broadband.

In the SSPP TL section, periodic sub-wavelength grooves are arranged in the metal microstrip lines with a period of $p = 2.5$ mm, a duty cycle of $dc = a/p = 0.6$, and a groove depth of $h = 4$ mm. The gap, $ga = 0.28$ mm, and width, $W_1 = 5$ mm, of the central strip are designed to achieve a 50 Ω impedance. The antenna adopts a single-port and tapered structure at the end.

In the radiation section, circular patches are placed near the SSPP TL. The front and rear backplanes are composed of circular patch arrays staggered in front and back. We set the period of single-side patch arrays, D, at 9.38 mm, and the distance between the patch center and the central axis at $d_1 = 6$ mm. The radius r is set at 4 mm.

3. Principle and analysis

3.1. SSPP TL analysis

We were able to confirm that periodic metallic grooves allow the surface plasmon mode to propagate at microwave frequencies. Figure 2 shows dispersion diagrams of single- and double-layer medium units with varying depths of groove. It is evident that with an increase in the frequency of the dispersion curve, β also increases, and gradually deviates from the light, where β represents the propagation constant. Closer to the asymptotic frequency, the alteration in the propagation constant is more dramatic. The figure shows that in contrast with the single-layer unit, double-layer units have a lower cutoff frequency, enabling the double-layer SSPP TL to confine EM on the surface more strongly than the single-layer TL. Moreover, the deeper the metal groove, the lower the cutoff frequency of the dispersion curve becomes. The depth, h, and structure of the model represent two important factors affecting the dispersion characteristics of the unit. We selected a dual-layer element with $h = 4$ mm to modulate the cutoff frequency at around 10 GHz.

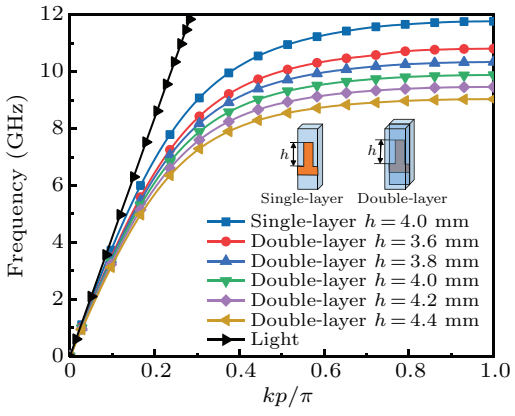


Fig. 2. Dispersion curves of the unit cell in SSPP TL.

In order to illustrate the characteristics of the TL, E-field distributions on double-end TLs at different frequency points in the *xoz* plane were simulated, as shown in Figs. 3(a) and 3(b). EM waves were transmitted through the TL at 8 GHz and 9.5 GHz to the other port. When the frequency is set to 10.5 GHz, it is clear that EM waves are strictly confined to the gradient part. The *S*-parameter in Fig. 3(c) shows that the cutoff frequency of TL is 10 GHz. Beyond the cutoff frequency, energy cannot be transmitted to the other end, clearly demonstrating the low-pass properties of TL.

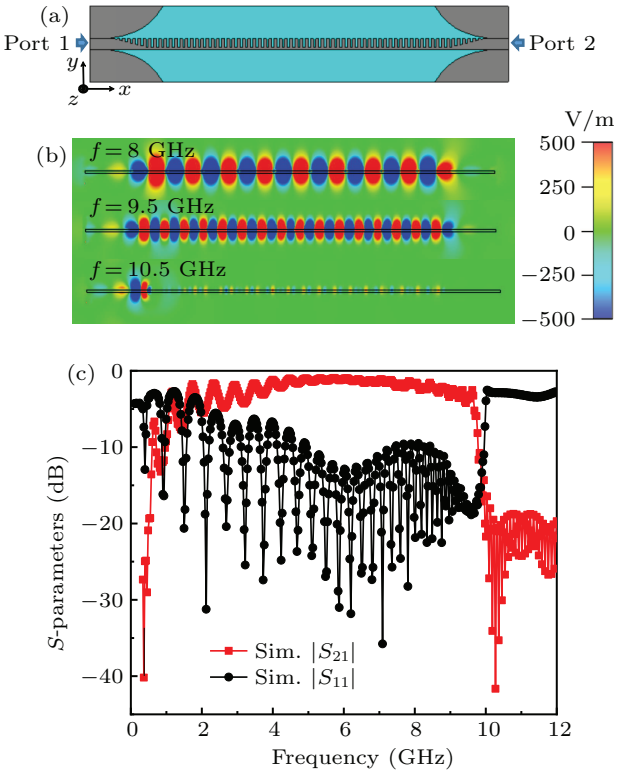


Fig. 3. Transmission characteristics of the SSPP TL. (a) Structural diagram of transmission line. (b) E-field distributions of the SSPP TL at 8 GHz, 9.5 GHz and 10.5 GHz in the *xoz* plane. (c) Simulated *S*-parameters of the SSPPs TL.

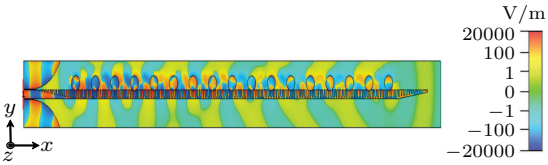


Fig. 4. Simulated electric-field distributions of the proposed SSPP LWA at 9 GHz.

Leaky-wave antenna usually adopts a dual-port structure to ensure that the EM waves transmitted to the end of the antenna can be absorbed, so that the reflected wave cannot affect the direction of radiation. The structure adopts a single-port and a tapered structure at the end, as shown in Fig. 1(b). Such a structure causes the SSPP wave mode to shift to the space wave mode, such that a small amount of EM waves reaching the end are radiated to reduce the impact of reflections on the original feeder electric field. In Fig. 4, we note that the energy along the TL decreases significantly along the *x*-direction.

3.2. Radiation element analysis

In order to radiate EM waves and form LWAs based on an SSPP TL, we need to disturb propagating surface waves by periodically placing radiating patches near the SSPP TL. If the radiation efficiency is high enough, the matching load can be removed, which not only reduces the antenna size but also decreases the influence of the end on the far field pattern of the patch arrays, and improves the realized gain.

The radiation element is a circular patch with isotropy, and the resonant frequency of the element is primarily determined by its size. Radiation efficiency can be improved by setting the element resonant frequency within the working bandwidth, so the radius r is set at 4 mm, based on the following expression:

$$r = \frac{k_{11}c}{2\pi\sqrt{\varepsilon_r}f}, \tag{1}$$

where k_{11} represents the eigenvalue of the TM_{11} mode, c is the velocity of the light in vacuum, and f is the center frequency.

In Fig. 1(d), an interleaved array of patches balances the front and rear of the far-field pattern so that the main radiation lobe can scan in the *xoy* plane of the antenna. Since the distance between front and rear is relatively close, there is no obvious deviation for the period D of periodic disturbance; placing patches on the upper and lower surface facilitates better coupling with the energy on the TL.

Methods such as mode balance,[18] impedance matching,[19,20] and loading asymmetric radiators[18,21,22] effectively suppress the open stop-band (OSB) effect. Moreover, as described in Ref. [14], the asymmetrical structure also helps to suppress the stop-band. There is no OSB problem in the antenna structure proposed in this paper. The beam-scanning characteristics of the antenna are realized via the feed phase difference in the SSPP TL. If we wish to realize radiation in the broadside direction, we need the patch to couple energy, and the adjacent phase difference is zero. Since the SSPP TL has different wave numbers at different frequencies, there must be a specific frequency point to realize zero phase difference between two adjacent patches. Once there is no phase difference between the patches, the radiation beam can access the broadside direction.

The asymmetric structure of the antenna effectively inhibits the generation of the stop-band, thereby removing the discontinuous scanning angle in the broadside, which is common in many other LWAs. The gap, d_1, between the patches and the TL only affects the coupling energy from the TL. These radiating patches couple EM waves from the SSPP TL through periodic disturbances, and radiate them into free space.

3.3. Analysis of beam scanning characteristics

The propagation constant of EM waves guided by a slow-wave structure is larger than that for a free space wave ($\beta_x > k_0$), and does not radiate. The design of the antenna is based on the principle of periodic disturbance,[10] which introduces an infinite number of spatial harmonics into the periodic traveling wave.

It is assumed that the EM waves propagate in the x direction. The fundamental mode is a slow wave ($\beta_0 > k_0$). However, there is always a certain harmonic (usually the -1^{st} harmonic) producing fast-wave radiation ($-k_0 < \beta_x < k_0$).

On this basis, the propagation constant along the x-axis can be expressed as

$$\beta_n = \beta_0 + 2\pi n/D, \quad n = 0, \pm1, \pm2, \ldots, \tag{2}$$

where D is the length of the periodic disturbance, and β_0 is the propagation constant in the fundamental mode. In order to achieve efficient frequency scanning, we generally adopt a space harmonic of $n = -1$ to realize beam scanning.

The deflection angle and propagation constant of the antenna satisfy the following relations:

$$\theta = \sin^{-1}(\beta_x/k_0), \tag{3}$$

where k_0 is the propagation constant in free space, θ is the included angle between beam direction and $+z$ axis, and β_x represents the propagation constant of the corresponding space harmonic.

Figure 5(b) shows the dispersion curves of the periodic element of the antenna along with the distribution of multiple harmonics. In the figure, A_1 (A_2), B_1 (B_2) and C_1 (C_2) represent the backward endfire, broadside radiation and forward endfire of harmonics, respectively:

$$\sin\theta_{\text{backward endfire}} = \beta_{-1}(f)/k_0,$$
$$\theta_{\text{backward endfire}} = 90^\circ, \quad (-k_0 = k_{A_1}), \tag{4}$$
$$\sin\theta_{\text{broadside}} = \beta_{-1}(f)/k_0,$$
$$\theta_{\text{broadside}} = 0^\circ, \quad (k_0 = k_{B_1}), \tag{5}$$
$$\sin\theta_{\text{forward endfire}} = \beta_{-1}(f)/k_0,$$
$$\theta_{\text{forward endfire}} = 90^\circ, \quad (k_0 = k_{C_1}), \tag{6}$$

where $\beta_{-1}(f)$ represents the dispersion curve of phase change with frequency change in the -1^{st} harmonic mode.

The dispersion characteristic data obtained via simulation is discrete. When deriving the formula, the fitted continuous curve is more conducive to the operation of the relationship between multiple harmonic dispersion curves. The reference values of key experimental parameters obtained by this operation are conducive to the design of the antenna. The frequency band of the -1^{st} harmonic radiation mode can be controlled by adjusting the size of the D parameter.

In order to more accurately calculate the disturbance cycle D value corresponding to the -1^{st} harmonic radiation

mode, MATLAB is used to fit the dispersion curve; the resulting expression is as follows:

$$\beta_0(f) = a_1 \times \mathrm{e}^{-(\frac{f-b_1}{c_1})^2} + a_2 \times \mathrm{e}^{-(\frac{f-b_2}{c_2})^2}, \tag{7}$$

where $a_1 = 1.824 \times 10^{19}$, $a_2 = 2.474 \times 10^5$, $b_1 = 23.61$, $b_2 = 52.75$, $c_1 = 2.217$, $c_2 = 17.76$.

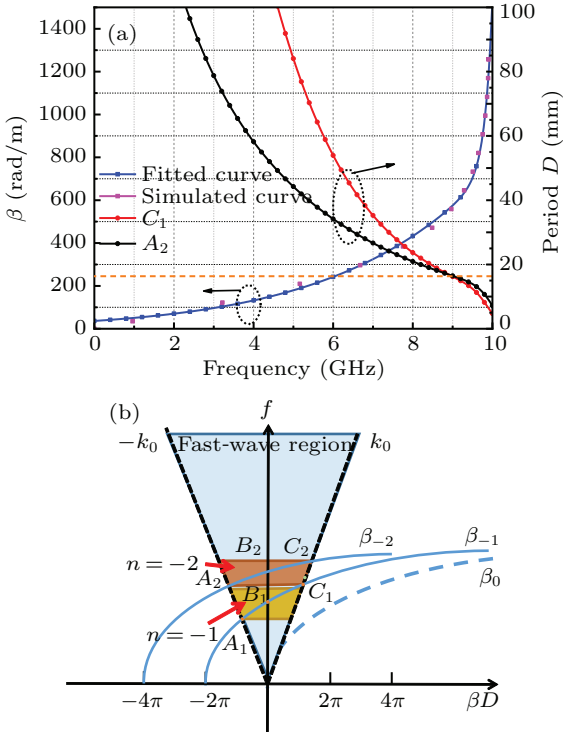


Fig. 5. Simulated results for harmonic dispersion and single-beam radiation conditions. (a) Diagram of fitting results and single-beam radiation conditions. (b) Harmonic dispersion curves of periodic elements.

The fitting curve in Fig. 5(a) is in good agreement with the simulation curve. The n^{st} harmonic radiation is expected to concentrate energy in a single lobe, which serves to improve the gain of the main lobe:

$$\begin{aligned}\beta_{f(A(n+1))} &= \beta_{0(f(A(n+1)))} - \frac{2(n+1)\pi}{D} \\ &= -k_{0A(n+1)} = -\frac{2\pi f_{(A(n+1))}}{c}, \end{aligned} \tag{8}$$

$$\beta_{fC(n)} = \beta_{0(fC(n))} - \frac{2n\pi}{D} = +k_{0C(n)} = \frac{2\pi f_{(C(n))}}{c}. \tag{9}$$

We can substitute this expression into the following:

$$f_{(A(n+1))} \geq f_{(C(n))}, \tag{10}$$

$$f_{(A(n))} \geq f_{(C(n-1))}, \tag{11}$$

where $\beta_{f(A(n+1))}$ represents the propagation constant of the $(n+1)^{\mathrm{st}}$ harmonic backward endfire, and $\beta_{f(C(n+1))}$ represents the propagation constant of the $(n+1)^{\mathrm{st}}$ harmonic forward endfire. Here, $k_{0C(n)}$ and $k_{0A(n)}$ represent the corresponding phase constant values of $C(n)$ and $A(n)$, respectively.

In Fig. 5(a), the radiation condition of the -1^{st} harmonic single beam can be obtained by substituting the fitted expression ($D \leq 16.8$ mm). By substituting the fitting curve expression, the relationship between D parameter and operating bandwidth can be calculated, which is also convenient for antenna design. The fitted continuous curve enables a more accurate prediction of the relationship between beam direction and frequency.

Different frequencies correspond to different propagation constants on the SSPP TL, resulting in different phases between the coupled patch arrays, culminating in the formation of different radiation directions in the far field. The expression obtained via fitting result in a more formulaic calculation, which makes the antenna radiation direction more accurate. By substituting into Eqs. (2), (3), and (7), we obtain frequency points corresponding to the theoretical radiation of the antenna. Theoretically, the frequency of backward, broadside, and forward endfire are 8.3 GHz, 9.1 GHz, and 9.6 GHz, respectively, while the actual results are 8.2 GHz, 9.2 GHz, and 9.6 GHz, respectively. The theoretical calculation results are in good agreement with the simulation results, which demonstrate that the dispersion curve expression obtained by the fitting curve can be fitted with the calculation results. As a result, the expression plays a guiding role in adjusting the working bandwidth of the antenna, and predicting the relationship between radiation direction and frequency. The fitting result further validates the feasibility of Eq. (7), and the validity of these equations is convenient in terms of determining the operating band for given structural parameters.

3.4. Analysis of high-frequency scanning rate implementation

In Fig. 6, the first shifted dispersion curve has a lower frequency and a larger slope change, while working in a wider bandwidth. The second shift has a higher frequency point with a smaller slope change, and backward to forward scanning can theoretically be realized.

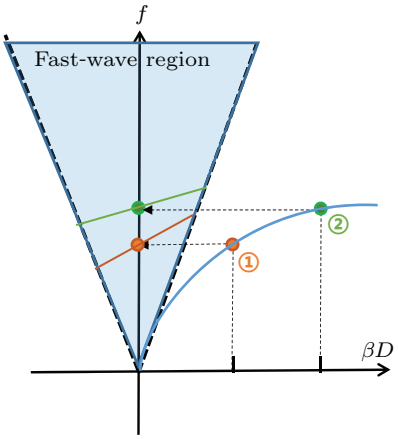


Fig. 6. Scanning rate comparison of two different momentum compensations for leaky-wave radiation.

Since the scanning rate of leaky-wave antennae is defined as the beam-scanning range divided by the frequency bandwidth (BW), a higher scanning rate can be realized by adjusting the phase shift close to the asymptotic frequency, resulting in a smaller-slope dispersion curve. By adjusting the D value, the operating frequency tends to be asymptotic, so that the antenna has the property of realizing wide-scanning-angle in a narrower bandwidth. In this way, the scanning rate (SR) can be improved.

4. Experimental validation

The proposed LWA was fabricated using standard printed circuit board (PCB) technology, and verified experimentally in an anechoic chamber. In Fig. 7, the vector network analyzer is used to measure the reflection coefficient, and the radiation mode is measured by the automatic turntable; the results show that the antenna can achieve reflection coefficients below −10 dB in the range of 8.3–9.8 GHz. The experimental results agree well with the simulated results. The frequency offset at the resonant frequency points may be caused by fabrication errors and different relative permittivity of the substrate, but the general trend remains consistent. Figure 7(b) also plots the relationship between realized gain and frequency, showing that the simulated peak gain of 11.6 dBi can be achieved at 9 GHz.

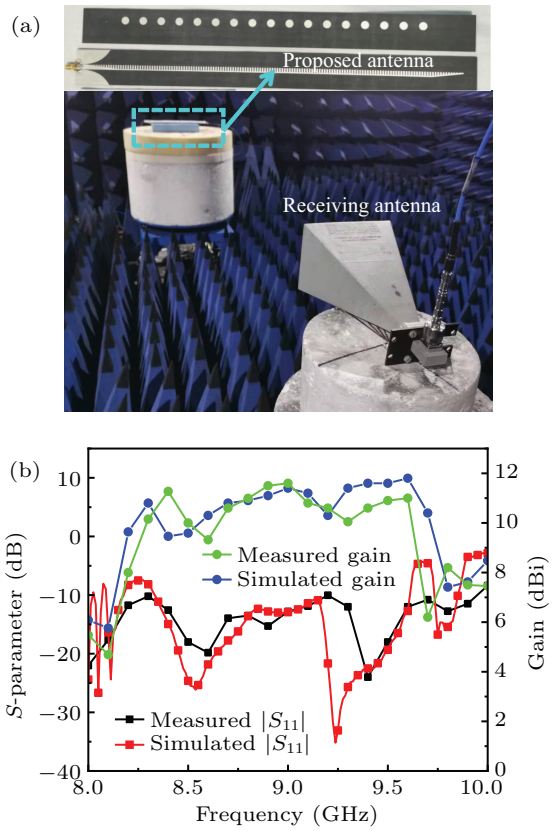


Fig. 7. Photograph of the fabricated antenna and performance parameters of the proposed antenna. (a) Photograph of the fabricated antenna under test. (b) Measured and simulated $|S_{11}|$ and gain.

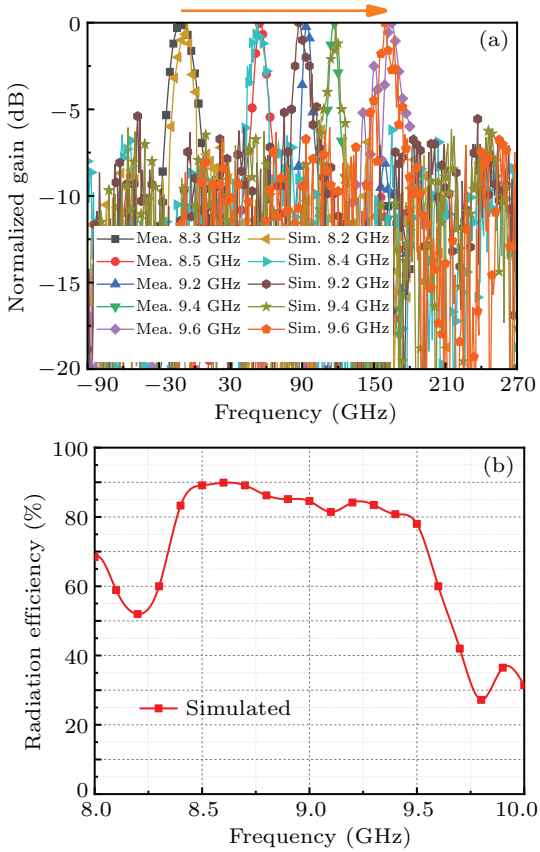


Fig. 8. Measured results of radiation patterns and simulated total efficiency. (a) Simulated and measured normalized E-plane radiation patterns at different frequencies. (b) Simulated total efficiency of the proposed LWA.

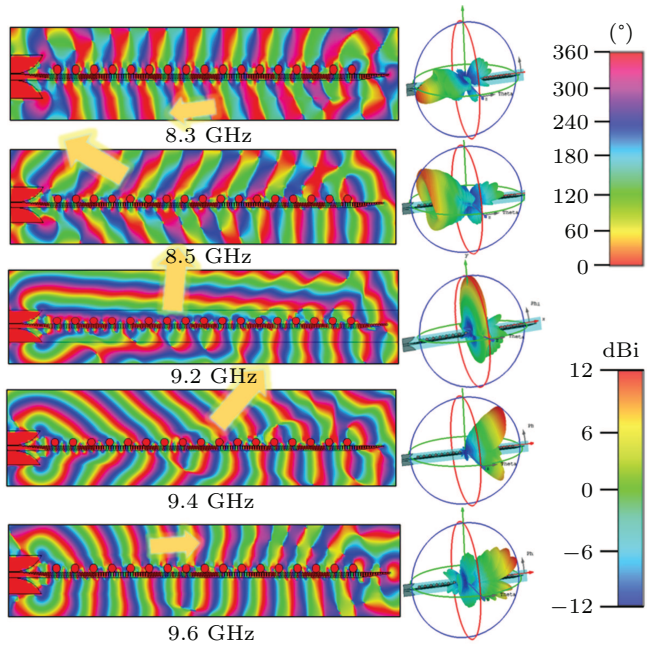


Fig. 9. Phase distribution of the proposed SSPP LWA and 3D far-field radiation at corresponding frequency points.

Furthermore, the measured radiation beam can scan from −13° to 162° within the frequency band of 8.2–9.8 GHz, while the simulated radiation beam can scan from −11° to 164° within the frequency band of 8.3–9.6 GHz, as shown in Fig. 8(a). In the experiment, frequency points corresponding to the five directions of backward endfire, backward, broad-

side, forward and forward maximum radiation angle are extracted and compared. The experimental and simulation results in the same direction can also be accepted for the processing and experimental operation methods, and the overall curves are in good agreement. The frequency scanning characteristics of the antenna radiation beam can be clearly seen from the figure.

As shown in Fig. 8(b), the simulated average efficiency of the antenna is as high as 81.4% within the working bandwidth, and the total radiation efficiency drops significantly in relation to the back and endfire directions.

Figure 9 shows the phase distribution of the proposed SSPP LWA, and 3D far-field radiation at corresponding frequency points. The antenna uses single-beam radiation in the operating frequency band, and exhibits outstanding radiating performance in both forward and backward directions.

Our antenna can achieve a large angle at a very high SR, with high radiation efficiency and high gain characteristics, demonstrating superior performance to other types of LWAs in almost all areas, as shown in Table 1.

Table 1. Comparison of various antennas of the same type.

Ref.	Total efficiency (%)	Average gain (dBi)	Scanning range (°)	BW (%)	Scanning rate
[10]	not mentioned	13.0	**18**	14.2	**1.27**
[11]	$\geq$ **40.2**	**7.9**	**123**	9.0	13.37
[13]	90 (average)	10.3	**83**	**54.0**	**1.54**
[14]	**26 (average)**	**3.0**	145	6.3	23.02
[14]	**67 (average)**	10.0	152	23	**6.6**
[15]	Not mentioned	11.5	**35**	3.0	11.37
[16]	80 (average)	10.9	129	**124.1**	**1.04**
[23]	$\geq$ **60**	15.9	**81**	33.3	**2.43**
[24]	not mentioned	13.0	**90**	27.1	**3.32**
[25]	70 (average)	9.8	55	75.0	**0.73**
Proposed	**81.4 (average)**	**10.9**	**176**	**14.5**	**12.12**

5. Conclusion

In this paper, we have proposed a single-beam leaky-wave antenna with wide-scanning-angle and high-scanning-rate based on an SSPP TL. A series of patches is periodically placed near the SSPP TL to couple the EM energy and radiate to free space. The experimental results are in agreement with the simulation and the proposed antenna can realize a high scanning rate of 12.12 while achieving a wide scanning angle from -12° to 164°. The fitted dispersion curve is conducive to calculate the condition of single beam radiation. The formula obtained by fitting discrete points provides effective guidance in terms of antenna design. Our leaky-wave antenna exhibits superior performance to all those demonstrated in similar works. With its high radiation efficiency, wide scanning angle range, and high scanning rate, the proposed shows great potential for application in radar and wireless communication systems.

Acknowledgements

Project supported by the National Natural Science Foundation of China (Grant Nos. 62171460 and 61801508), the Natural Science Basic Research Program of Shaanxi Province, China (Grant Nos. 2020JM-350, 20200108, 20210110, and 2020022), the Postdoctoral Innovative Talents Support Program of China (Grant Nos. BX20180375, 2019M653960, and 2021T140111).

References

[1] Kianinejad A, Chen Z N and Qiu C W 2017 *IEEE Trans. Antennas Propag.* **65** 681
[2] Li S J, Li Y B, Zhang L, *et al*. 2021 *Laser Photonics Rev.* **15** 2000449
[3] Han B W, Li S J, Li Z Y, *et al*. 2021 *Opt. Express* **29** 19643
[4] Li Z Y, Li S J, Han B W, *et al*. 2021 *Adv. Theory Simul.* **4** 2100117
[5] Li S J, Li Y B, Li H, *et al*. 2020 *Annalen der Physik* **532** 2000020
[6] Barnes W L, Dereux A and Ebbesen T W 2003 *Nature* **424** 824
[7] Tian D, Xu R, Peng G, Li J, Xu Z, Zhang A and Ren Y 2018 *IEEE Antennas Wirel. Propag. Lett.* **17** 837
[8] Jaiswal R K, Pandit N and Pathak N P 2018 *IEEE Photonic. Tech. L.* **31** 218
[9] Wei D, Li J, Yang J, Qi Y and Yang G 2018 *IEEE Antennas Wirel. Propag. Lett.* **17** 1566
[10] Kong G S, Ma H F, Cai B G and Cui T J 2016 *Sci. Rep.* **6** 29600
[11] Xu S, *et al*. 2019 *IEEE Antennas Wirel. Propag. Lett.* **18** 1386
[12] Wang M, Ma H F, Tang W X, *et al*. 2019 *Phys. Rev. Appl.* **12** 014036
[13] Liao D, Zhang Y and Wang H 2018 *IEEE Antennas Wirel. Propag. Lett.* **17** 1238
[14] Zhang G, Zhang Q F, Chen Y F and Murch R D 2019 *IEEE Trans. Antennas Propag.* **68** 2531
[15] Guan D F, Zhang Q F, You P, *et al*. 2018 *IEEE Trans. Antennas Propag.* **66** 3747
[16] Wang J, Zhao L, Hao Z C and Cui T J 2020 *IEEE Trans. Antennas Propag.* **68** 7652
[17] Ma H F, Shen X, Cheng Q, *et al*. 2014 *Laser Photonics Rev.* **8** 146
[18] Otto S, RenningsA, Solbach K and Caloz C 2011 *IEEE Trans. Antennas Propag.* **59** 3695
[19] Paulotto S, Baccarelli P, Frezza F and Jackson D R 2009 *IEEE Trans. Antennas Propag.* **57** 1894
[20] Yang N, Caloz C and Wu K 2010 *IEEE T. on Microw. Theory* **58** 2619
[21] Tang X L, Zhang Q, Hu S, Zhuang Y, Kandwal A, Zhang G and Chen Y 2017 *Sci. Rep.* **7** 11685
[22] Otto S, Al-Bassam A, Rennings A, Solbach K and Caloz C 2012 *IEEE Antennas Wirel. Propag. Lett.* **11** 612
[23] Wei D J, Li J Y, Yang J J, Qi Y X and Yang G W 2018 *IEEE Antennas Wirel. Propag. Lett.* **17** 1566
[24] Jidi L R, Cao X Y, Zhu X W and Zhu B W 2018 *Prog. Electrom. Res. Le.* **77** 117
[25] Yin J Y, Zhang Q, Zhang H C, Liu Y Q, Li Y B, Wan X and Cui T J 2016 *IEEE Trans. Antennas Propag.* **64** 5181
[26] Chang K 2000 *RF and Microwave Wireless Systems* pp. 111–148